JTTEE5 16:610–618
DOI: 10.1007/s11666-007-9116-6
1059-9630/$19.00 © ASM International

Influence of the Powder Size Distribution on the Microstructure of Cold-Sprayed Copper Coatings Studied by X-ray Diffraction

T. Kairet, M. Degrez, F. Campana, and J.-P. Janssen

(Submitted March 9, 2007; in revised form August 13, 2007)

Two copper powders were deposited with CGT3000 cold-gas dynamic spray system on aluminum substrates. Mechanical properties have been studied using microhardness, nanoindentation, and bond strength measurements. The deposition efficiency has also been studied. The x-ray diffraction patterns allow the characterization of the microstructure such as grain size, strain in the coating, and dislocation densities. Both powders and coatings have been fully characterized. Three methods have been used to interpret the x-ray patterns: the Warren-Averbach method, the Hall-Williamson (H-W) method, and the modified H-W method. A comparison between the state of the powders before and after deposition will give an insight on the metallurgical processes that take place during the formation of the coating. The influence of the grain size distribution will also be discussed.

Keywords cold-gas dynamic spraying, copper, Hall-Williamson, Warren-Averbach, x-ray diffraction

1. Introduction

The cold-gas dynamic spray process leads to the build up of a coating by accelerating fine powders (5–25 μm in diameter) to supersonic speeds in a Laval nozzle. The powder particles impact the surface with a speed ranging from 500 to 1200 m/s and bond to the surface when a critical value of impact speed is reached. During the impact, severe plastic deformation and high strain rates allow the formation of adiabatic shear bands at the interface between the impinging particle and the substrate. Several authors (Ref 1, 2) have linked the value of the critical speed for bonding to the onset of these adiabatic shear bands. Borchers et al. (Ref 3) have observed grain refinement and changes in the copper microstructure at the interface between grains. Fine elongated grains and possibly some recrystallized grains have also been identified.

This article is an invited paper selected from presentations at the 2007 International Thermal Spray Conference and has been expanded from the original presentation. It is simultaneously published in *Global Coating Solutions, Proceedings of the 2007 International Thermal Spray Conference*, Beijing, China, May 14-16, 2007, Basil R. Marple, Margaret M. Hyland, Yuk-Chiu Lau, Chang-Jiu Li, Rogerio S. Lima, and Ghislain Montavon, Ed., ASM International, Materials Park, OH, 2007.

T. Kairet and **M. Degrez**, Matière & Matériaux, Université Libre de Bruxelles, Rue de l'Industrie 24, Nivelles, 1400, Belgium; and **F. Campana** and **J.-P. Janssen**, Advanced Coating, S.A., Liege, Belgium. Contact e-mail: tkairet@ulb.ac.be.

The powder size distribution will have a crucial importance on the quality of the coating. The process is essentially influenced by the kinetic energy transferred to the particles. A different size distribution of the powder means that the kinetic energy is distributed differently. Mechanical properties such as bond strength and hardness will be affected by the size distribution. Other properties like deposition efficiency (DE) and porosity all depend on the size distribution.

X-ray diffraction has been used for several years to characterize microstructure of metals and materials. This method identifies different phases of materials present if the volume of each phase is sufficient to be detected. X-ray diffraction also allows characterizing the microstructure of the materials. The shape, the asymmetry, and the position of the diffraction peaks are influenced by several factors:

- Dislocations
- Twins and staking faults
- Grain boundaries
- Subgrain boundaries
- Vacancies
- Inclusions
- Misfits between different phases

Developments of this method allow identifying how diffraction patterns are affected by these defects. Ungár et al. (Ref 4, 5) have developed the classical Hall-Williamson (H-W) method and Warren-Averbach (W-A) method to take into account the strain anisotropy of the x-ray peaks diffraction and the influence of dislocations and planar faults on peak broadening.

This study aims at describing how two different copper powders with a different grain size distribution and a

different microstructure build up into the coating with different mechanical properties. Three spraying conditions have been compared for their mechanical properties. X-ray diffraction will allow interpreting some results.

2. Experimental Method

2.1 Materials and Spray Conditions

Two commercially available powders (Fig. 1) from different powder suppliers have been used; both are gas-atomized powders. These powders have a different size distribution (Fig. 2). The size distribution and volume distribution have been measured with the Occhio optical device (OCCHIO. S.A. (Ref 6)). The substrate is a commercially available aluminum which has been polished. Figure 2 shows that powder A is finer than powder B. Substrate properties are summarized in Table 1. The hardness has been measured using a Vickers test. A load of 10 kg was applied on the aluminum substrate. The oxygen content is given by the suppliers. The oxygen content of powders A and B is 0.25 wt.% and 0.02 wt.%, respectively.

The spray conditions are summarized in Table 2. The main gas used is nitrogen in a CGT installation (Cold Gas Technology. GmbH) with the CGT standard nozzle. Three values of stagnation pressure and gas temperatures have been used. Spray conditions have been chosen to maximize the effect of impact speed and to obtain a coating with sufficient thickness to measure their properties. Other spray conditions (Table 3) have been determined by the industrial installation used in Advanced Coating S.A. (Ref 7).

2.2 Coating Characterization

Microhardness measurements have been done using a Vickers indenter with an applied load of 300 g (2.94 N). The load increase is 0.4 N/s. The Vickers hardness value is obtained by using

$$\text{Vickers hardness} = \frac{0.189 \cdot F}{d^2} \quad [\text{N/mm}^2]$$

where F is the load applied and d is the diagonal of the indentation.

The bond strength was measured with a standard pull-off test on aluminum substrates.

Nanoidentation tests were performed using a Hysitron TriboIndenter with a Berckovich tip on the cross section of the coating. Cold mounting was used to prepare the samples. The copper coatings were polished with 2 μm diameter MgO, with the OP-Solution, and a solution with 0.3 μm alumina suspensions. Several polishing tests were attempted to evaluate surface preparation effects on the measurements. The load function applied on the surface was a trapezoidal function with steady increase up to 6000 μN in 5 s followed by a constant load value for 2 s and a decrease from 6000 μN to 0 in 5 s. The mechanical response of the coating allowed measuring the hardness of the coating and it's Young's Modulus. Measurements were taken in which the tip of the indenter has been placed at the interface between the substrate and the copper coating and a series of 10 indentations spaced by 10 μm from each other have been done. On each coating, three profiles have been made and the data is presented as an average hardness with the corresponding standard deviation. No interesting information has been obtained by doing nanoindentation on either substrate.

Before x-ray diffraction, the coatings have been mechanically polished to remove surface roughness on the surface. Samples have been analyzed in a Siemens D5000 with a Cu anode operating at 40 kV and 40 mA. The $K_{\alpha 2}$ component of the Cu radiation was eliminated by software subtraction. The x-ray patterns have been done between 40 and 140 °C. The angular step is 0.02° and each step was measured during 40 s. The x-ray peaks of the first five peaks have been used for the H-W analysis with the following miller hkl index: 111, 200, 220, 311, and 222. For the W-A procedure, the fifth peak was not used. Its shape was insufficiently resolved for the W-A method.

The coatings have been etched with a solution composed of 50% of concentrated hydrogen peroxide and 50% of ammoniac.

2.3 Peak Profile Analysis Method

The x-ray diffraction pattern is the convolution between the ''pure'' material broadening effect and the instrumental broadening. It is necessary to subtract the instrumental broadening to the measured profile (Ref 8).

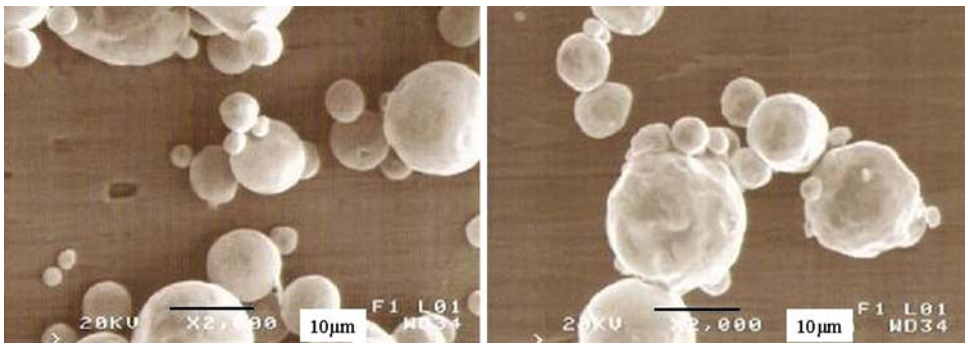

Fig. 1 SEM images. Left: powder A; Right: powder B

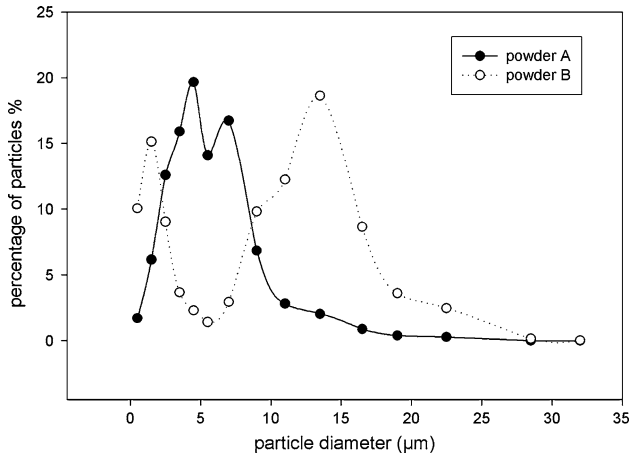

Fig. 2 Measured frequency size distribution of both powders

Table 1 Substrate properties before spraying

	Al substrate
Average roughness	0.2 μm Ra
Average hardness	67.3 $HV_{10\ kg}$

Table 2 Variable spray conditions (stagnation pressure P_0 and temperature T_0)

Spray conditions	N_2 gas stagnation pressure, bars	N_2 gas stagnation temperature, °C
1	22	320
2	26	420
3	30	520

Table 3 Constant spray parameters

Powder feed rate	40 g/min
Gun speed	397 mm/s
Standoff distance	40 mm
Used nozzle	CGT standard
Main gas	N_2

The measured full width at half maximum (FWHM) is the sum between the "pure" FWHM and the instrumental FWHM.

$$I(2\theta)^{\text{measured}} = I(2\theta)^{\text{pure}} \times I(2\theta)^{\text{instrumental}}$$
$$\text{FWHM}^{\text{measured}} = \text{FWHM}^{\text{pure}} + \text{FWHM}^{\text{instrumental}} \quad \text{(Eq 1)}$$

The procedure uses a LaB_6 references samples to model the effect of instrumental broadening. The instrumental FWHM and the shape factor (m) are fitted with a second-order polynomial function. This allows the synthesis of instrumental FWHM at any desired angle and the asymmetrical line instrumental profile at any desired angle with a split Pearson VII function.

$$\text{FWHM}^2_{\text{instrumental}} = a \cdot \tan^2(\theta) + b \cdot \tan(\theta) + c$$
$$m_{\text{instrumental}} = d \cdot (2\theta)^2 + e \cdot (2\theta) + f \quad \text{(Eq 2)}$$

The use of this approach requires only one standard regardless of peak positions and the analyzed specimen. It minimizes the error of standard parameters by averaging over a large number of reflections.

The classical H-W method is described by Calla et al. (Ref 9). It gives the value of the crystallite size D and the microstrain. By assuming that the main source of strain in the crystal is associated with dislocations and planar faults, the classical H-W can be improved. The modified H-W plot takes into account the effect of strain anisotropy by the introduction of the dislocation contrast factor, C. The contrast factor depends on the relative orientation between Burger vector, line vector, the diffraction vector, and the crystal elastic constants. The average dislocation contrast factor for FCC metals can be written as:

$$\bar{C} = \bar{C}_{h00} \cdot (1 - q \cdot H^2) \quad \text{(Eq 3)}$$

where

$$H^2 = \frac{h^2k^2 + h^2l^2 + k^2l^2}{(h^2 + k^2 + l^2)^2} \quad \text{(Eq 4)}$$

In the case of copper (Ref 10), $\bar{C}_{200} = 0.304$ is a calculated value based on an average of edge and screw dislocations with the burger vector $\vec{b} = \frac{a}{2}\langle 110\rangle$ on slip plane {111}. q depends on the edge or screw character of the dislocations. By comparing the experimental value of q with the calculated value, it is possible to establish the dislocation character in the coating. For copper, theory gives a value of $q = 1.68$ for pure edge dislocations and a value of $q = 2.37$ for pure screw dislocations. The modified H-W equation that includes planar faults is:

$$\Delta K - \beta' \cdot W(\vec{g}) = \frac{0.9}{D_{\text{H-W}}} + A_1 \cdot \left[\left(K\bar{C}^{1/2}\right)\right] + A_2 \cdot \left[\left(K\bar{C}^{1/2}\right)\right]^2 \quad \text{(Eq 5)}$$

The planar fault density β' includes the effect of twinning and faulting and the $W(\vec{g})$ coefficient are given by Warren (Ref 11). $D_{\text{H-W}}$ is the crystallite size in the sense of the H-W method and A_1, A_2 are fitted constants. The modified H-W plot corresponds to the plot of ΔK as a function of $K\bar{C}^{1/2}$ where,

$$\Delta K = \frac{2\cos(\theta) \cdot \text{FWHM}}{\lambda}, \quad K = \frac{2\sin(\theta)}{\lambda} \quad \text{(Eq 6)}$$

The W-A method allows a peak analysis without any hypothesis on the shape of the peak. This method is based on the analysis of the real part of the Fourier coefficient analysis $A(n)$. The basic approach is to dissociate the contribution of size and distortion on the Fourier coefficient,

$$\ln(A(n)) = \ln\left(A^S(n)\right) + \ln\left(A^D(n)\right) \quad \text{(Eq 7)}$$

where $A^S(n)$ and $A^D(n)$ are, respectively, the size and distortion contribution to the real part of the Fourier coefficient.

The modified W-A equation that takes into account planar fault is:

$$\ln(A(L)) + L\beta' W(g) \cong -\frac{L}{D_{\mathrm{W-A}}} - \rho^* B L^2 \ln\left(\frac{R_e}{L}\right)\left(K^2\bar{C}\right) + O\left(\left(K^2\bar{C}\right)^2\right) \quad \text{(Eq 8)}$$

where $D_{\mathrm{W\text{-}A}}$ is the crystallite size in the sense of the W-A method, ρ* is the ''formal'' dislocation density, R_e is the outer cut off radius, $L = n \cdot a_3$ is the Fourier variable, and B is linked to the burger vector of the slip system (Ref 11). Higher-order terms in the W-A equation can be added. The modified W-A plot corresponds to the plot of $\ln(A(n))$ as a function of $K^2\bar{C}$.

The classical H-W method does not take into account the effect of strain anisotropy. Points in the H-W plot are scattered around the fitted line. It makes it difficult to interpret the data physically.

The introduction of the contrast factor allowed modifying the H-W plot to improve the fitting procedure (Fig. 3).

The W-A method is more precise than the H-W method, it used the whole peak to get the information. The peak-broadening analysis of the real part of the Fourier coefficient gives information on the crystallite size, the dislocation density ρ*, the outer cut off radius and the higher-order terms give information on dislocations organization. The imaginary part of the Fourier coefficient is associated with the polarization of the dislocation structure. The accuracy of the peak measurement limited the use of more than four peaks for the W-A analysis (Ref 10) and prevented the interpretation of higher-order terms in the analysis. An example of the W-A modified plot is shown in Fig. 4 the result of the fitting procedure. Second-order terms were included in the calculation as the support terms but not interpreted. Each method yields a different crystallite size from which some authors get size distribution of the crystallites (Ref 5). In this study, the differences in crystallite sizes between both powders, as illustrated in Table 4, yield different information on the mechanical properties of the powders.

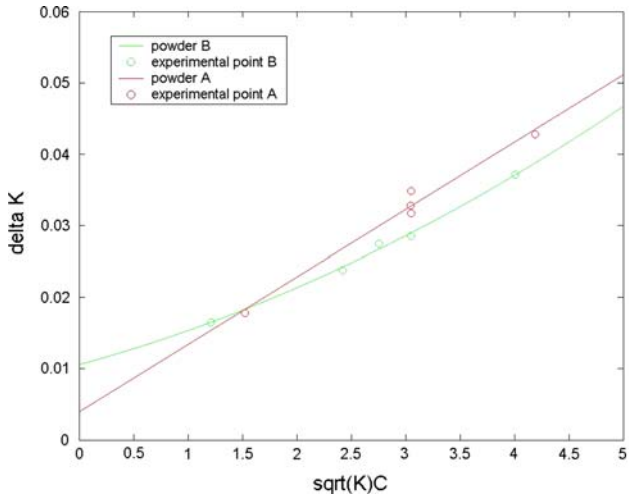

Fig. 3 Modified H-W plot for powders A and B

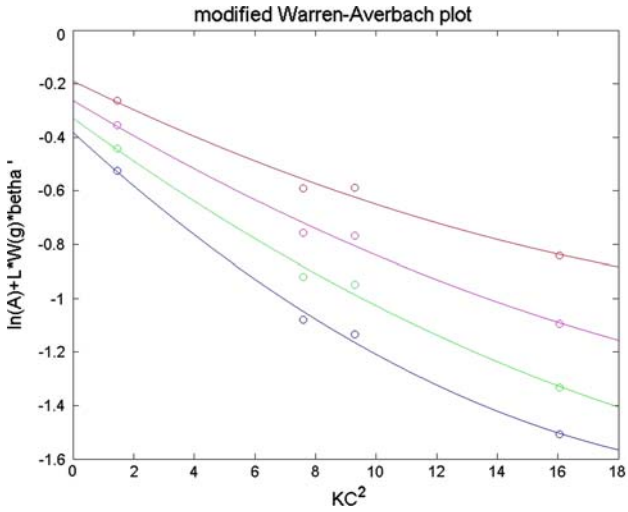

Fig. 4 Modified W-A plot for the coating sprayed with powder A at 520 °C and 30 bars for four values of the Fourier length L

3. Results

All the spray-deposition experiments were realized in Advanced Coating S.A.

3.1 Powder Analysis

The data in Table 4 compiles the results from the classical and modified H-W and the W-A method. Both powders have a similar dislocation density but the crystallite size is, on the whole, bigger in powder A than in powder B.

3.2 Deposition Efficiency

Figure 5 shows the evolution of the DE on the aluminum substrate. Powder A shows a sharp increase in DE when the spray conditions favor a higher particle speed. Powder B yields a good DE at low velocity on aluminum.

Table 4 X-ray diffraction results on the copper powders A and B

	Powder A	Powder B
H-W classical		
Diameter (D), nm	168	120
Microstrain, %	0.1	0.15
H-W modified		
Diameter ($D_{\mathrm{H\text{-}W}}$), nm	223	85
Density SFE & twin: β′, %	0.269	0.25
q	2.01	2.37
W-A modified		
Diameter ($D_{\mathrm{W\text{-}A}}$), nm	105	97.11
Formal dislocation density (ρ*), m^{-2}	1.37×10^{15}	1.71×10^{15}
Radius (R_e), nm	67.6	73
Density SFE & twin: β′, %	0.5	0

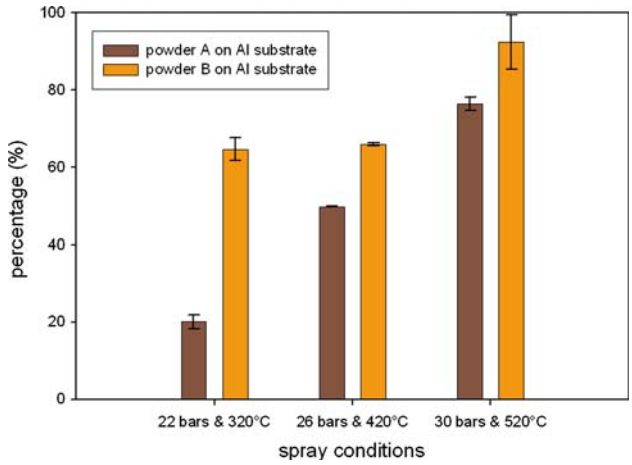

Fig. 5 Deposition efficiency of the Cu powders on the Al substrate

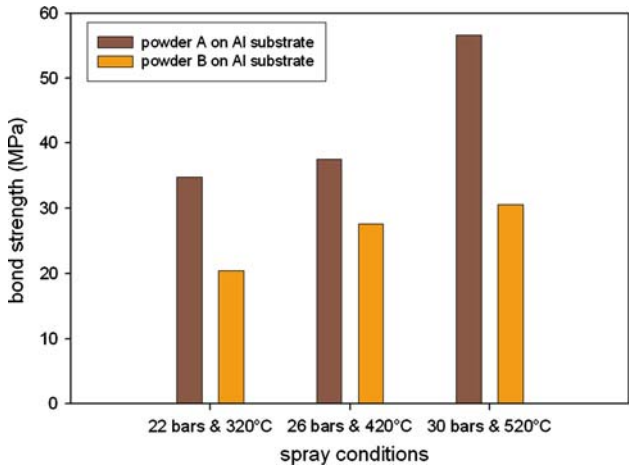

Fig. 6 Bond strength of the coatings on the Al substrate measured by a pull-off test

3.3 Mechanical Properties of Cu Coatings on Al Substrate: Microhardness and Bond Strength

Figure 6 shows the evolution of the bond strength as a function of the spray conditions. The powder A shows higher bond strength than powder B.

No standard deviation data is presented for the bond strength because only one measurement was made in some cases. The data indicates a trend for bond strengths.

Figure 7 shows the evolution of microhardness when the powder's speed is increased. Powder A exhibits higher hardness values than powder B. Each measurement is an average value of ten indentations done on the coating with the corresponding standard deviation. The coating sprayed with a stagnation pressure of $P_0 = 22$ bars and a stagnation temperature of $T_0 = 320$ °C using powder A was too thin to perform microhardness testing. The nanoindentation has provided a measurement of the hardness on thin coatings.

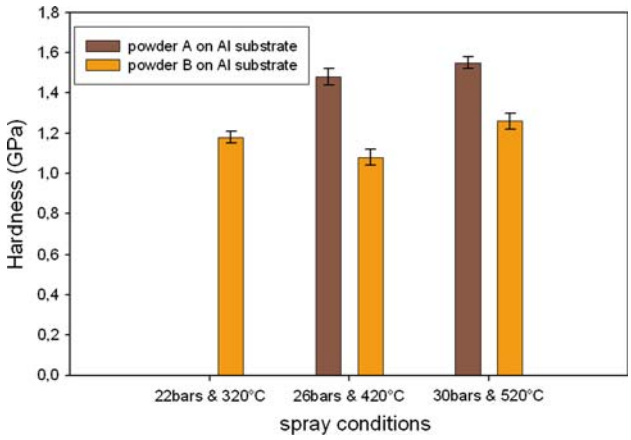

Fig. 7 Microhardness values on the Al substrate

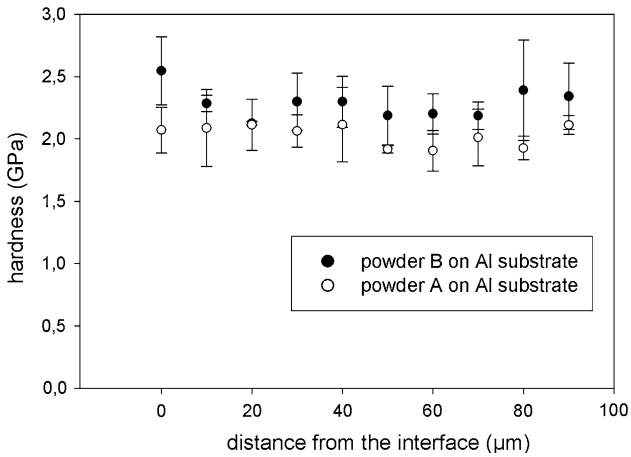

Fig. 8 Comparison between the hardness profile of both coatings on the Al substrate with the spray condition $P_0 = 30$ bars and $T_0 = 520$ °C

3.4 Hardness Profiles: Influence the Powder's Size Distribution

Figure 8 shows that powder B has led to a harder coating than powder A. Powder B being coarser; it had to undergo less deformation during impact. Powder A, with a higher impact speed, has generated a higher dislocation density.

3.5 Coating Analysis X-ray Diffraction Analysis

Figures 9 and 10 are optical micrographs of both etched copper coatings sprayed with both powders under spray conditions 3. The boundaries between deformed particles show up clearly with the application of the etchant on both coatings. In the case of the coating made with powder A, some powder grains show an internal cell substructure that is not visible on powder B. Both coatings have also been analyzed with x-ray diffraction; results are listed in Table 5. In Table 6, are listed the properties of copper coatings sprayed with a stagnation gas pressure of 22 bars and a stagnation temperature of 320 °C.

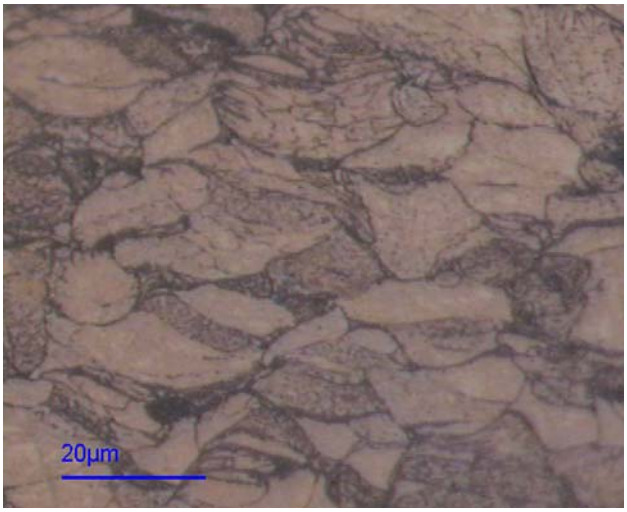

Fig. 9 Etched coating sprayed with powder A at 520 °C and 30 bars

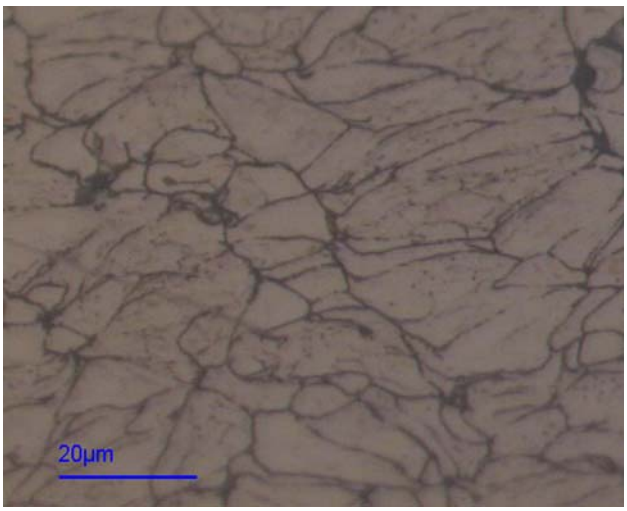

Fig. 10 Etched coating sprayed with powder B at 520 °C and 30 bars

4. Discussion

X-ray diffraction will give an average view on the microstructural changes in a large volume of materials. The highly localized deformation's contribution to the peak broadening at the interface between powder particles cannot be distinguished clearly from the global deformation of the powder grain. The average numbers, given in previous tables, show average changes in the microstructure during the coating formation. These numbers give trends in the coating.

4.1 Powder Comparison

Powder A has a smaller size distribution than powder B therefore, at fixed sprayed conditions, powder A will be faster than powder B. It has a high sensitivity to spray conditions. It is likely that powder A will deform more than powder B upon impact.

Each diffraction method used to characterize the copper powders has shown that powder A has a larger crystallite size than powder B (Table 4). The formal value of the dislocation densities for powder A is lower than powder B. The value of the crystallite size is important to determine the mechanical properties of the coatings. A material with a large crystallite size will be more ductile than a powder with a fine nanostructure. Both powders are gas-atomized. The raw material is melted and then atomized in a controlled atmosphere. This process involves very high quench rates. Planar faults seem to be present in more important quantities in powder A. The presence of twins as a consequence of static recrystallization could be an explanation for these planar faults. The difference in quench rates between the powders is the most significant factor that leads to these differences even if it was not visible on the optical micrographs. The value of q for powder A is 2.01. Therefore, powder A has about 50% of edge and screw dislocations where powder B has essentially screw dislocations.

Table 5 X-ray diffraction results on the copper coating made with both powders sprayed at 520 °C and 30 bars

	Coating with powder A	Coating with powder B
H-W classical		
Diameter (D), nm	67	78
Microstrain, %	0.2	0.17
H-W modified		
Diameter ($D_{H\text{-}W}$), nm	51.7	64.3
Density SFE & twin:β′, %	0.7	0.21
q	2.37	2.37
W-A modified		
Diameter ($D_{W\text{-}A}$), nm	57.3	53
Formal dislocation density (ρ*), m^{-2}	4.43×10^{15}	3×10^{15}
Radius (R_e), nm	40	61.6
Density SFE & twin: β′, %	0	0

Table 6 X-ray diffraction results on the copper coating made with both powders sprayed at 320 °C and 22 bars

	Coating with powder A	Coating with powder B
H-W classical		
Diameter (D), nm	85.4	75.8
Microstrain, %	0.22	0.17
H-W modified		
Diameter ($D_{H\text{-}W}$), nm	66	68
Density SFE & twin: β′, %	0	0.49
q	2.37	2.37
W-A modified		
Diameter ($D_{W\text{-}A}$), nm	56.56	52.31
Formal dislocation density (ρ*), m^{-2}	4.4×10^{15}	3.47×10^{15}
Radius (R_e), nm	36	51
Density SFE & twin: β′, %	0	0

It is likely that powder A has a different thermal history then powder B. The cooling rate of powder A after atomization seems to be slower than that of powder B. It allowed larger crystallite size to form. Another aspect supports this idea: Powder A has a larger oxide content than powder B. A slow cooling rate would allow a larger oxide shell to build up around the powder particles. This difference comes from the specific aspect of the powder suppliers' manufacturing process that has not been elucidated by this study.

4.2 Influence on the DE and the Mechanical Properties

As observed on Fig. 4, the DE of powder A is lower than that of powder B. It has been argued by Li et al. (Ref 12) that the high oxide content implies an increase in the critical velocity for bonding. Hence, powder A with its high oxide content has a lower DE than powder B.

Microhardness values are shown in Fig. 7. The fine size distribution of powder A yields higher microhardness values compared to powder B. The higher number of grain boundaries between the deposited particles hinders the plastic deformation during indentation, hence it increases the hardness value. Powder A has also a higher surface to volume ratio; therefore, more oxide impurities on the particles' surface are trapped in the coating. This will also hinder plastic deformation during indentation.

The crystallite size of powder A, measured by x-ray diffraction, is smaller than powder B and adiabatic shear bands have formed more extensively and grain refinement was more important. Due to the non-uniform microstructure, grain refinement has occurred in the shear bands while the center of the particle has kept its initial crystallite size. This explains the difference in nanohardness observed in the coating in Fig. 8. The coating sprayed with powder A has a lower nanohardness than the one sprayed with powder B. The x-ray data also shows the crystallite size between spray conditions 1 and 3 is not very different. This implies that spray conditions have not influenced significantly the formation of the shear bands, in both cases. This also agrees with the fact that the nanohardness profiles are not influenced by spray conditions. With both of these spray conditions, the deposited material has reached its critical velocity. The powder grains that have not reached the critical velocity are not in the coating. The use of spray conditions 3 has induced recrystallization. Planar faults are detected with these spray conditions where fewer are detected with spray condition 1. These types of faults induce a reduction in the apparent crystallite size compared to the ''true crystallite'' size. The powder particles' temperature upon impact could explain the presence of these planar faults by increasing the amount of recrystallization in the coating.

4.3 Influence of the Spray Conditions

Spray conditions will influence the impact speed and temperature of the powder particles. High-impact velocity improves the bonding between the coating and the substrate as shown in Fig. 6. Powder A being finer than powder B, its impact velocity is higher than powder B. The oxide shell around the powder does not allow a good quality contact between the substrate and the powder particle. Powder A also has a larger crystallite size than powder B, hence, it will be more ductile upon impact. Once the oxide shell around powder A is broken, the higher ductility of the powder allows a better contact between the substrate and the coating. X-ray diffraction did not distinguish the different effects of spray conditions 1 and 3. The diffraction was done on the top layer of the surface. This layer is the last layer deposited and all particles are above the critical speed. They all undergo the same deformation. X-ray diffraction yield average information from a large surface while adiabatic shear bands are very local by nature. It is likely that it is not possible to obtain information on the influence of spray conditions on the shear bands in the coating by this method.

4.4 Influence of the Powder on the Dislocation Type in the Coating

Copper coatings show a decrease in the crystallite size compared with the powder. As it was expected, dislocations have multiplied during deformation and a small-scale cell structure has formed. Copper is a material with a relatively low stacking fault energy compared to other FCC material like Ni and Al; therefore, the coating microstructure is non uniform. Powder A with the smallest initial powder size distribution underwent the most significant grain refinement. The initial low dislocation of powder A density has allowed extensive dislocation multiplication in the coating. Powder B is initially rich in dislocation jogs and boundaries that are obstacles to dislocation movements compared to powder A. All coatings contain essentially screw dislocations since the value of $q = 2.37$. The presence of dislocation loops has been detected by Borchers et al. (Ref 13) and they could explain the presence of this high density of screw dislocations. The contribution of the defect type to broadening is based on the decay of strain field around the defect. This allows a classification of the defect contribution. It is not possible to distinguish the contribution of these loops to the broadening. As explained by Kuzel (Ref 14), the high screening by the dislocations in the coating modifies the displacement fields of some defects. Dislocation loops have not been clearly identified by this method. They still play a crucial role in dislocation organization during deformation. Work by Shehadeh et al. (Ref 15) has used dislocation dynamics to simulate shock loading in copper. They have shown that the use of Frank-Read dislocations loops as a generation source of dislocations leads to the formation of band like dislocation cell walls that coincide with the slip plane. This mechanism is associated with the double cross slip of screw dislocations in the material. This explains the presence of essentially a majority of screw dislocations in the coating. They have the ability to cross slip. This is also supported by Chen et al. (Ref 16).

4.5 Influence of the Powder on the Coating's Dislocation Density

The main differences between the coatings are the dislocations density and the value of R_e. The spray conditions do not seem to have influence on the crystallite size. Ductile powder with an initially low dislocation density gives a coating with a very high dislocation density and a small radius R_e. The physical meaning of R_e is more complex. It's meaning is related to the restricted random distribution of dislocation introduced by Wilkens and is linked to the length scale within which the distribution is random (Ref 14). This parameter can be taken as a measure of correlation in dislocation distribution. This small value of R_e implies a high correlation between dislocations in the cell walls in the shear bands. For powder A, the length to which dislocations are distributed randomly is small. The dipole character of dislocations in powder A is more significant (Ref 17). The initial high ductility of powder A allows the dislocations to reorganize on a larger scale. With powder A, it is likely that more dislocations are organized in the cell walls than in the case of powder B. This powder is rich in obstacles to dislocation motion. Since powder B is also coarser than powder A, it will have a smaller impact velocity. This powder will not deform as largely has powder A and dislocations will not have sufficient energy to integrate the cell walls in the shear bands and they will be distributed more uniformly in the coating. The difference in dislocation density ρ^* is also a consequence of the powders' initial microstructure. Powder B with more obstacles to dislocation motion and multiplication will keep a lower dislocation density in the coating. This explains the higher values observed for R_e and lower dislocation density ρ^* in the case of powder B.

5. Conclusion

- The mechanical properties are influenced by the properties of the initial powder. X-ray diffraction patterns show that different powders' microstructures yield different coating microstructures and mechanical properties. The smaller crystallite size of powders yield a higher ductility, hence thermal softening during the formation of adiabatic shear bands lead to an improved bond with the substrate.
- Spray condition favors an increase in the impact velocity hence an increase in bond strength. The highly localized shear band deformation during the powder's impact is not fully captured by the x-ray diffraction. Therefore, no significant differences between the spray conditions have been observed by x-ray diffraction.
- The oxide content of the powder has reduced the efficiency of the deposition but the fine size distribution has allowed a high impact velocity to break off the oxide shell and to get a clean contact between pure materials.

It appears that the most significant influence on the mechanical properties comes from the differences in the original powder microstructure. The size distribution of the powder will determine the impact velocity while the original microstructure of the powder will play a role on the plastic deformation during impact. Both are linked but rarely discussed simultaneously.

The use of x-ray diffraction line profile analysis enables to access the features of the microstructure of the powder before and after spraying. This opens the perspective to discuss the optimization of the process in relationship with the powder state before spraying.

Acknowledgments

This work was funded by the Walloon Government (DGTRE) and the European Social Fund (ESF). n° «EPH3310300R0392»/«215299».

References

1. M. Grujicic, J.R. Saylor, D.E. Beasley, W.S. DeRosset, and D. Helfritch, Computational Analysis of the Interfacial Bonding between Feed-Powder Particles and the Substrate in the Cold Gas Dynamic Spray Process, *Appl. Surf. Sci.*, 2003, **219**(1), p 211-327
2. H. Assadi, F. Gärtner, T. Stoltenhoff, and H. Kreye, Bonding Mechanism in Cold Gas Spraying, *Acta Mater.*, 2003, **51**, p 4379-4394
3. C. Borchers, F. Gärtner, T. Stoltenhoff, H. Assadi, and H. Kreye, Microstructural and Macroscopic Properties of Cold Spayed Copper Coatings, *J. Appl. Phys.*, 2003, **93**(12), p 10064-10070
4. T. Ungár, S. Ott, P.G. Sanders, A. Borbely, and J.R. Weertman, Dislocation, Grain Size and Planar Faults in Nanostructured Copper Determined by High Resolution X-ray Diffraction and a New Procedure of Peak Profile Analysis, *Acta Mater.*, 1998, **46**, p 3693-3699
5. T. Ungár, Dislocation Densities, Arrangements and Character from X-ray Diffraction Experiments, *Mater. Sci. Eng. A*, 2001, **309-310**, p 14-22
6. http://www.occhio.be/en/homepage, contact distributor: Advanced Coating S.A., 7 rue de l'avouerie, 4000 Liège
7. T. Kairet, G. Di Stefano, M. Degrez, F. Campana, and J.-P. Janssen, Comparison Between Coatings from two Different Copper Powders: Mechanical Properties, Hardness and Bond Strength, *Building on 100 Years of Success: Proceedings of the 2006 International Thermal Spray Conference*, B.R. Marple, M.M. Hyland, Y.C. Lau, R.S Lima, and J. Voyer, Eds., May 15-18, 2006 (Seattle, WA, USA), ASM International
8. D. Balzar, Profile Fitting of X-ray Diffraction Lines and Fourier Analysis of Broadening, *J. Appl. Cryst*, 1992, **25**, p 559-570
9. E. Calla, D.G. McCartney, and P.H. Williams, Effect of Heat Treatment on the Structure and Properties of Cold Sprayed Copper, *Thermal Spray 2005: Explore its Surface Potential*, May 2-4, 2005 (Basel, Switzerland), ASM International, p 170
10. T. Ungár, I. Groma, and M. Wilkens, Asymmetric X-ray Line Broadening of Plastically Deformed Crystals. II. Evaluation Procedure and Application to [001]-Cu Crystals, *J.Appl. Cryst.*, 1989, **22**, p 26-34
11. B.E. Warren, X-ray Studies of Deformed Metals, *Prog. Metal Phys.*, 1959, **8**, p 147-201
12. C.-J. Li, W.-Y Li, and H. Liao, Examination of the Critical Velocity for Deposition of In Cold Spraying, *J. Thermal Spray Technol.*, 2006, **15**(2), p 212-222
13. C. Borchers, F. Gärtner, T. Stoltenhoff, and H. Kreye, Formation of Persistent Dislocation Loops by Ultra-High Strain-Rate Deformation During Cold Spraying, *Acta Mater.*, 2005, **53**, p 2991-3000

14. R. Kuzel, Dislocation Line Broadening, *Z. Kristallogr. Suppl.*, 2006, **23**, p 75-80
15. M.A. Shehadeh, H.M. Zbid, and T. Diaz de la Rubia, Multiscale Dislocations Dynamics Simulations of Shock Compression in Copper Single Crystals, *Int. J. Plast.*, 2005, **21**, p 2369-2390
16. H. Chen, Y.L. Yao, J.W. Kysar, I.C. Noyan, and Y. Wang, Fourier Analysis of X-ray Micro-Diffraction Profiles to Characterize Laser Shock Peened Metals, *Int. J. Solids Struct.*, 2005, **42**, p 3471-3485
17. E. Schafler, K. Simon, S. Bernstorff, P. Hanak, G. Tichy, T. Ungár, and M.J. Zehetbauer, Second Order Phase Transformation of the Dislocation Structure During Plastic Deformation Determined by In Situ Synchrotron X-ray Diffraction, *Acta Mater.*, 2005, **53**, p 315-322